

Supersolid phase of extended Bose-Hubbard model with artificial gauge field

K. Suthar,^{1,2} Rukmani Bai,^{1,3} Soumik Bandyopadhyay,^{1,3} Sukla Pal,^{1,4} and D. Angom¹

¹Physical Research Laboratory, Ahmedabad - 380009, Gujarat, India

²Instytut Fizyki imienia Mariana Smoluchowskiego,

Uniwersytet Jagielloński, ulica Łojasiewicza 11, 30-348 Kraków, Poland

³Indian Institute of Technology Gandhinagar, Palaj, Gandhinagar - 382355, Gujarat, India

⁴Department of Physics, Centre for Quantum Science, and Dodd-Walls Centre for Photonic and Quantum Technologies, University of Otago, Dunedin, New Zealand

(Dated: April 30, 2019)

We examine the zero and finite temperature phase diagram of the extended Bose-Hubbard model on a square optical lattice. To study various quantum phases and their transitions we employ single-site and cluster Gutzwiller mean-field theory. We have observed that the Mott insulator phase vanishes above a critical value of nearest-neighbour interaction and the supersolid phase occupies a larger region in the phase diagram. We show that the presence of artificial gauge field enlarges the domain of supersolid phase. The finite temperature destroys the crystalline structure of the supersolid phase and thereby favours normal fluid to superfluid phase transition. The presence of an envelope harmonic potential demonstrates coexistence of different phases and at $z k_B T \geq U$, the supersolidity of the system is destroyed.

I. INTRODUCTION

Ultracold atomic systems have played an important role in the study of quantum many-body systems. In particular, the novel experimental developments in manipulating ultracold atoms in optical lattices have led to the realization of new quantum states and quantum phase transitions in strongly correlated systems [1, 2]. In recent years, there has been a surge of interest in understanding the supersolid (SS) phase which is characterized by the simultaneous appearance of a crystalline and an off-diagonal long-range orders [3, 4]. This phase breaks two continuous symmetries: the phase invariance of the superfluid (SF) and translational invariance to form crystal. Although the SS phase was predicted in liquid ⁴He a long time ago [5, 6], the experimental observation of supersolidity in liquid ⁴He remains elusive [7–9]. However, the quest for SS phase has gained new impetus following the remarkable theoretical insights and experimental achievements in ultracold atoms in optical lattices, which are excellent quantum many-body systems to observe SS phase as these are clean and controllable. Recently, the characteristic signature of SS phase has been observed in ultracold atoms [10–14] and this phase may emerge by tuning the bosonic interactions of different length scales [15]. The existence and stability of SS phase have been confirmed in an optical cavity [16].

On theoretical front, the existence of SS phases has been studied using the extended Bose-Hubbard model (eBHM) with nearest-neighbour (NN) repulsions. However, the SS phase is fragile and previous studies have demonstrated that SS phase does not exist with NN interaction for square [17, 18] and honeycomb [19, 20] lattices. The checkerboard SS phase is unstable and the system undergoes phase separation into SF and solid phases [21]. However, dipolar interaction, which decays as the inverse cube of the distance, stabilize the SS phase [22, 23]. The SS phase can also be stabilized by tuning the anisotropy of the dipolar interaction [24, 25]. This phase has been explored in various lattice systems, such as one-dimensional (1D) chain [26, 27], two-dimensional (2D) square [21, 22, 28–31], triangular [32–37],

honeycomb [19, 20], kagome [38], bilayer lattice of dipolar bosons [39], and three-dimensional (3D) cubic lattice [30, 40–42].

In this work we investigate theoretically the presence of SS phase in 2D square optical lattice with long-range interaction and artificial gauge field. The long-range interaction can be realized with the dipolar ultracold atoms [43, 44]. And, it is possible to introduce artificial gauge field with lasers [45–48]. We show that the combined effect of the long-range interaction and artificial gauge field increases the domain of the SS phase. In particular, we examine the effect of magnetic flux quanta on the SS-SF phase boundary in the presence of the NN interaction. Furthermore, to relate with experimental realizations, we incorporate the effects of thermal fluctuations arising from finite temperature. For our studies we use the single-site and cluster mean-field theories.

The paper is organized as follows. In Sec. II we introduce the model considered in our study and describe theoretical approach employed. Here we provide description of the single-site, cluster and finite temperature Gutzwiller (GW) mean-field theories. The ground-state phase diagrams and study of dipolar atoms in the confining potential are presented in Sec. III. Finally, we conclude with the key findings of the present work in Sec. IV.

II. THEORETICAL METHODS

A. Extended Bose-Hubbard model

Consider a system of bosonic atoms with long-range interactions in a 2D square optical lattice in the presence of synthetic magnetic field. The temperature of the system is low such that all the atoms occupy the lowest Bloch band. Such a system is well described by eBHM, and the Hamiltonian of

the model is

$$\begin{aligned} \hat{H}_{\text{eBHM}} = & - \sum_{p,q} \left(J_x \hat{b}_{p+1,q}^\dagger \hat{b}_{p,q} + J_y \hat{b}_{p,q+1}^\dagger \hat{b}_{p,q} + \text{H.c.} \right) \\ & + \sum_{p,q} \hat{n}_{p,q} \left[(\epsilon_{p,q} - \mu) + \frac{U}{2} (\hat{n}_{p,q} - 1) \right] \\ & + \sum_{\langle \xi \xi' \rangle} V_{\xi, \xi'} \hat{n}_\xi \hat{n}_{\xi'}, \end{aligned} \quad (1)$$

where $p(q)$ is the lattice site index along $x(y)$ direction, $\hat{b}_{p,q}^\dagger$ ($\hat{b}_{p,q}$) is the bosonic operator which creates (annihilates) an atom at the lattice site (p, q) , $\hat{n}_{p,q} = \hat{b}_{p,q}^\dagger \hat{b}_{p,q}$ is the boson number operator, J_x and J_y are the tunneling or hopping strength between two NN sites along x and y directions, respectively, $\epsilon_{p,q}$ is the offset energy arising due to the presence of external envelope potential, μ is the chemical potential, and $U > 0$ is the on-site interatomic interaction. Here ξ is a combination of lattice indices in 2D, that is, $\xi \equiv (p, q)$ and $\xi' \equiv (p', q')$ are neighbouring sites to ξ . The long-range interaction $V_{\xi, \xi'}$ for $V_1 - V_2$ model is given by

$$V_{\xi, \xi'} = \begin{cases} V_1 & \text{if } |\mathbf{r}_{pq} - \mathbf{r}_{p'q'}| = a, \\ V_2 & \text{if } |\mathbf{r}_{pq} - \mathbf{r}_{p'q'}| = \sqrt{2}a, \\ 0 & \text{otherwise,} \end{cases} \quad (2)$$

where a is the lattice spacing, $\mathbf{r}_{pq} = (pa, qa)$ is the lattice site coordinates. The parameters $V_1 \geq 0$ and $V_2 \geq 0$ are the NN and next NN (NNN) interactions, respectively. The other type of long-range interaction is the dipolar interaction. In the experiments of ultracold quantum gases, long-range interaction can arise from either electric or magnetic dipole moments. To examine the effect of the dipolar interaction, assume that the dipoles are polarized along z -axis. So that the atoms experience an isotropic repulsive dipole-dipole interaction in the xy plane. The long-range dipole interaction $V_{\xi, \xi'}$ in the 2D square lattice is

$$V_{\xi, \xi'} = \begin{cases} \frac{Va^3}{|\mathbf{r}_{pq} - \mathbf{r}_{p'q'}|^3} & (p, q) \neq (p', q'), \\ 0 & (p, q) = (p', q'). \end{cases} \quad (3)$$

Since the dipolar interaction falls off as the inverse cube of the distance, the dipolar interaction is $\{V, V/2\sqrt{2}, V/8, V/5\sqrt{5}, \dots\}$ for the NN, NNN, third, fourth neighbours, and so on. In theoretical studies the range of dipolar interaction is considered only upto certain neighbours. For the present work, we consider the first two terms, though simple this encapsulates all the observable effects of the dipole interactions in the system.

B. Artificial gauge field

The long-range interaction in the above Hamiltonian, Eq. (1), is characteristic or inherent to the internal state of the atomic species. In terms of the many-body physics, the nature of the correlation can further be modified through the intro-

duction of artificial gauge field. The presence of the artificial gauge field modifies the Hamiltonian to

$$\begin{aligned} \hat{H}_{\text{eBHM}} = & - \sum_{p,q} \left(J_x e^{i2\pi\alpha q} \hat{b}_{p+1,q}^\dagger \hat{b}_{p,q} + J_y \hat{b}_{p,q+1}^\dagger \hat{b}_{p,q} + \text{H.c.} \right) \\ & + \sum_{p,q} \hat{n}_{p,q} \left[(\epsilon_{p,q} - \mu) + \frac{U}{2} (\hat{n}_{p,q} - 1) \right] \\ & + \sum_{\langle \xi \xi' \rangle} V_{\xi, \xi'} \hat{n}_\xi \hat{n}_{\xi'}, \end{aligned} \quad (4)$$

where the strength of the magnetic field is reflected in the number of flux quanta per plaquette $\alpha = (e/\hbar) \int dr. \mathbf{A}(\mathbf{r})$. Here, $0 \leq \alpha < 1$, and $\mathbf{A}(\mathbf{r})$ is the vector potential which gives rise to synthetic magnetic field $\mathbf{B} = \nabla \times \mathbf{A}$. In the presence of the synthetic magnetic field, atoms acquire a $2\pi\alpha$ phase when they hop around a plaquette. This results into a phase shift in the hopping strength of the model. Physically, the synthetic magnetic field introduces a force on the atoms which is equivalent of the Lorentz force on a charged particle in the presence of external magnetic field. The system is then a charge neutral analogue of the quantum Hall system in condensed matter systems. For the present study, we consider Landau gauge, where the vector potential $\mathbf{A}(\mathbf{r}) = -By\hat{x}$. Hence, for the homogeneous system, at zero magnetic field the system possesses the translational invariance along both axes, whereas in the presence of magnetic field the system preserves the invariance only along the x -axis of the lattice.

C. Gutzwiller mean-field theory

To study the ground-states of the systems described by the model Hamiltonians in Eq. (1) and (4) and their properties we use single-site Gutzwiller mean-field (SGMF) and cluster Gutzwiller mean-field (CGMF) theories. The later is the extension of SGMF which incorporates the correlation within a cluster of neighbouring sites exactly. In the SGMF theory [49–51], the bosonic operators are expanded about their expectation values as

$$\hat{b}_{p,q} = \phi_{p,q} + \delta\hat{b}_{p,q}, \quad (5a)$$

$$\hat{b}_{p,q}^\dagger = \phi_{p,q}^* + \delta\hat{b}_{p,q}^\dagger. \quad (5b)$$

Therefore, the product of the creation and annihilation operators which occurs in the hopping term can be written as

$$\hat{b}_{p,q}^\dagger \hat{b}_{p',q'} \approx \phi_{p,q}^* \hat{b}_{p',q'} + \hat{b}_{p,q}^\dagger \phi_{p',q'} - \phi_{p,q}^* \phi_{p',q'}, \quad (6)$$

where second order terms in the fluctuation $\delta\hat{b}_{p,q}$ are neglected. Here, $\phi_{p,q} = \langle \hat{b}_{p,q} \rangle$ is the SF order parameter of the system. Using above approximation in the Hamiltonian,

Eq. (4), the single-site mean-field Hamiltonian is

$$\begin{aligned} \hat{H}_{p,q}^{\text{MF}} = & - \left[J_x e^{i2\pi\alpha q} \left(\phi_{p+1,q}^* \hat{b}_{p,q} - \phi_{p+1,q}^* \phi_{p,q} \right) \right. \\ & + J_y \left(\phi_{p,q+1}^* \hat{b}_{p,q} - \phi_{p,q+1}^* \phi_{p,q} \right) + \text{H.c.} \left. \right] \\ & + \left[(\epsilon_{p,q} - \mu) + \frac{U}{2} (\hat{n}_{p,q} - 1) \right] \hat{n}_{p,q} \\ & + \sum_{\langle \xi, \xi' \rangle} V_{\xi, \xi'} \hat{n}_{\xi} \hat{n}_{\xi'}, \end{aligned} \quad (7)$$

and the total Hamiltonian of the system is

$$\hat{H}_{\text{MF}} = \sum_{p,q} \hat{H}_{p,q}^{\text{MF}}. \quad (8)$$

Here, the neighbouring lattice sites are coupled through $\phi_{p,q}$, the SF order parameter. And therefore the eigenstate of the entire lattice is the products of single-site states. Accordingly, the many-body wave function of the ground state of the system is given by the Gutzwiller ansatz

$$|\Psi\rangle = \prod_{p,q} |\psi\rangle_{p,q} = \prod_{p,q} \left(\sum_{n=0}^{N_b} c_n^{(p,q)} |n\rangle_{p,q} \right), \quad (9)$$

where $|\psi\rangle_{p,q}$ is the single-site ground state, N_b is the number of occupation basis or maximum number of bosons at each lattice site, $|n\rangle_{p,q}$ is the occupation or Fock state of n bosons occupying the site (p, q) and $c_n^{(p,q)}$ is the probability amplitude or coefficients of the occupation state. The normalization of the wave function leads to the normalization of $c_n^{(p,q)}$ at each lattice site as $\sum_n |c_n^{(p,q)}|^2 = 1$. Using the above ansatz the SF order parameter $\phi_{p,q} = \langle \Psi | \hat{b}_{p,q} | \Psi \rangle$ is obtained as

$$\phi_{p,q} = \sum_{n=0}^{N_b} \sqrt{n} c_{n-1}^{(p,q)*} c_n^{(p,q)}. \quad (10)$$

Similarly, the occupancy of each lattice site $n_{p,q} = \langle \Psi | \hat{b}_{p,q}^\dagger \hat{b}_{p,q} | \Psi \rangle$ is

$$n_{p,q} = \sum_{n=0}^{N_b} n |c_n^{(p,q)}|^2. \quad (11)$$

The two parameters $\phi_{p,q}$ and $n_{p,q}$, together serve to define the quantum phases of the system. In the MI phase, ϕ is zero and $n_{p,q}$ is integer commensurate. The density-wave (DW) phase also has zero ϕ , and $n_{p,q}$ integer but incommensurate with long-range crystalline order. In contrast, for the SF phase ϕ is non-zero and $n_{p,q}$ has real value, and both the parameters are commensurate across the lattice. The SS phase too has non-zero ϕ and real $n_{p,q}$, but both of these have long-range crystalline order.

Although, the quantum phases of the system can be defined based on ϕ and $n_{p,q}$, these do not serve as good markers of the phase boundaries. To identify the phase boundaries, the

trends in the energy of the system is a reliable measure. From the mean-field Hamiltonian, Eq. (7), the total energy of the system $E = \langle \Psi | \hat{H}_{\text{MF}} | \Psi \rangle$ is obtained as a sum of the single-site energies $E_{p,q} = \langle \Psi | \hat{H}_{p,q}^{\text{MF}} | \Psi \rangle$. It is to be mentioned here that the computation of the total energy $E = \sum_{p,q} E_{p,q}$ is also required to obtain the ground state in the SGMF theory. As in the SGMF theory for eBHM, E is minimized self consistently with the Eqs. (10) and (11).

In the CGMF theory, a lattice of dimension $K \times L$ is partitioned into W clusters of size $M \times N$, that is $W = (K \times L)/(M \times N)$ [52–58]. Then, the hopping terms of the model are decomposed into two types. One is the exact term which corresponds to hopping within the cluster, and the other is the inter-cluster hopping between lattice sites which lie on the boundary of two neighbouring clusters. The latter is defined by coupling through the mean-field or the SF order parameter. The Hamiltonian of a cluster is

$$\begin{aligned} \hat{H}_C = & - \sum'_{p,q \in C} \left(J_x e^{i2\pi\alpha q} \hat{b}_{p+1,q}^\dagger \hat{b}_{p,q} + J_y \hat{b}_{p,q+1}^\dagger \hat{b}_{p,q} + \text{H.c.} \right) \\ & + \sum_{p,q \in \delta C} \left(J_x e^{i2\pi\alpha q} (\phi_{p+1,q}^c)^* \hat{b}_{p,q} + J_y (\phi_{p,q+1}^c)^* \hat{b}_{p,q} + \text{H.c.} \right) \\ & + \sum_{p,q \in C} \left[(\epsilon_{p,q} - \mu) \hat{n}_{p,q} + \frac{U}{2} \hat{n}_{p,q} (\hat{n}_{p,q} - 1) \right] \\ & + \sum_{\langle \xi, \xi' \rangle \in C} V_{\xi, \xi'} \hat{n}_{\xi} \hat{n}_{\xi'} + \sum_{\langle \xi, \xi' \rangle \in \delta C} V_{\xi, \xi'} \hat{n}_{\xi} \langle \hat{n}_{\xi'} \rangle, \end{aligned} \quad (12)$$

where the model parameters J_x , J_y , U and $V_{\xi, \xi'}$ are defined like in SGMF and prime in the first summation indicates that the $(p+1, q)$ and $(p, q+1)$ lattice sites are also within the cluster. Here, δC in the second summation represents the lattice sites at the boundary of the clusters and $(\phi_{p,q}^c) = \sum_{p',q' \notin C} \langle \hat{b}_{p',q'} \rangle$ is the SF order parameter at the lattice site which lies at the boundary of neighbouring cluster. Like hopping, the long-range interaction term also has two contributions, one is within the cluster which is exact, and the other is inter-cluster interaction at the boundary which is defined through the mean occupancy $\langle \hat{n}_{\xi'} \rangle$. The matrix elements of \hat{H}_C are, then, calculated in terms of the cluster basis states

$$|\Phi_c\rangle_\ell = \prod_{q=0}^{N-1} \prod_{p=0}^{M-1} |n_p^q\rangle, \quad (13)$$

where $|n_p^q\rangle$ is the occupation number basis at the (p, q) lattice site, and $\ell \equiv \{n_0^0, n_1^0, \dots, n_{M-1}^0, n_0^1, n_1^1, \dots, n_{M-1}^1, \dots, n_{M-1}^{N-1}\}$ is the index quantum number to identify the cluster state. After diagonalizing the Hamiltonian, we can get the ground state of the cluster as

$$|\Psi_c\rangle = \sum_{\ell} C_{\ell} |\Phi_c\rangle_{\ell}, \quad (14)$$

where C_{ℓ} are components of the eigenvector, and naturally satisfy the normalization condition $\sum_{\ell} |C_{\ell}|^2 = 1$. The ground state of the entire $K \times L$ lattice, like in SGMF, is the direct

product of the cluster ground states

$$|\Psi_{\text{GW}}^c\rangle = \prod_k |\Psi_c\rangle_k, \quad (15)$$

where k is the cluster index and varies from 1 to $W = (K \times L)/(M \times N)$. The SF order parameter ϕ , like in Eq. (10), can be computed in terms of the cluster states. The average occupancy of the k th cluster can also be computed similarly.

D. Finite temperature Gutzwiller mean-field theory

At finite temperature, the thermal fluctuations modify the properties of the system, and observable properties are the thermal averages. To calculate the thermal averages we need the entire eigenspectrum. So, in the SGMF, we retain the entire energy spectrum $E_{p,q}^l$ and the eigenstates $|\psi\rangle_{p,q}^l$ obtained from the diagonalization of the single-site Hamiltonian $\hat{H}_{p,q}^{\text{MF}}$ in Eq. (7). Then, we evaluate the single-site partition function of the system

$$Z = \sum_{l=1}^{N_b} e^{-\beta E^l}, \quad (16)$$

where $\beta = 1/k_B T$ and T is the temperature of the system. At finite T , the region in the phase diagram with $\phi = 0$ and the real commensurate occupancy $\langle \hat{n}_{p,q} \rangle$ is identified as the normal fluid (NF) phase. Similarly, in the CGMF, the partition function is defined in terms of all the eigenvalues E_k^l and eigenfunctions $|\Psi_c\rangle_k^l$ of each k th cluster from all the W clusters.

From the definition of the partition function, in the SGMF, the thermal average of $\phi_{p,q}$ is

$$\langle \phi_{p,q} \rangle = \frac{1}{Z} \sum_{i=0}^{N_b} \sum_{p,q} \langle \psi | \hat{b}_{p,q} e^{-\beta E^i} | \psi \rangle_{p,q}^i, \quad (17)$$

where $\langle \dots \rangle$ represents the thermal averaging. Similarly, the occupancy or the density at finite T is defined as

$$\langle \langle \hat{n}_{p,q} \rangle \rangle = \frac{1}{Z} \sum_{i=0}^{N_b} \sum_{p,q} \langle \psi | \hat{n}_{p,q} e^{-\beta E^i} | \psi \rangle_{p,q}^i. \quad (18)$$

The average occupancy is $\langle n \rangle = \sum_{p,q} \langle \langle \hat{n}_{p,q} \rangle \rangle / (K \times L)$. These definitions can be extended to the CGMF by replacing the single-site states and energies with that of the cluster.

III. RESULTS AND DISCUSSIONS

The standard BHM shows two phases, the incompressible Mott insulator (MI) phase corresponding to commensurate integer filling, and the compressible SF phase which has finite ϕ . The SF-MI quantum phase transition was observed by tuning the depth of the optical lattice [59]. In eBHM, the introduc-

tion of the NN interaction changes the phase diagram through the emergence of two more phases. First is the DW, which sandwiches the MI lobes at low values of NN interaction, and second is the SS phase, it occurs as envelope around the DW lobes. In this work, we first examine the phase diagram for the homogeneous systems. We, then, study the impact of artificial gauge field on the phase diagram by considering $\alpha = 1/2$. For comparison with experimental realizations, we also study with envelope potential.

Besides $\phi_{p,q}$ and $\langle \hat{n}_{p,q} \rangle$, the relative average occupancy Δn is another order parameter which can distinguish the DW and SS phases from MI and SF phases. For a $K \times L$ lattice and SGMF method it is defined as

$$\langle \Delta n \rangle = \frac{1}{K \times L} \sum_{p,q} |\langle \hat{n}_{p,q} \rangle - \langle \hat{n}_{p+1,q} \rangle|. \quad (19)$$

The similar expression can be defined for CGMF method. For the DW and SS phases $\langle \Delta n \rangle$ is nonzero, and in particular, it is integer and real for the DW and SS phases, respectively. But, for MI and SF phases $\langle \Delta n \rangle$ is zero as $\langle \hat{n}_{p,q} \rangle$ is uniform.

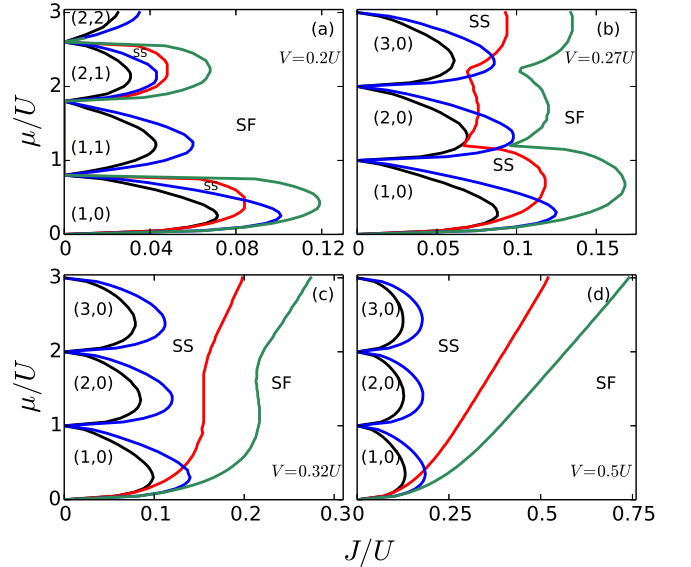


FIG. 1. The phase diagrams of the eBHM with uniform hopping amplitude ($J_x = J_y = J$) for $V/U = 0.2, 0.27, 0.32,$ and 0.5 (a-d). The densities of the MI and DW phases are shown in the parenthesis. The plots show the phase boundaries for two cases $\alpha = 0$ and $\alpha = 1/2$. For the former case, the black line indicates the MI-SF or the DW-SS phase boundaries and the red line shows the SS-SF phase boundary. For the $\alpha = 1/2$ case, the blue line marks the MI-SF or DW-SS phase boundary and green line corresponds to the SS-SF boundary.

A. Homogeneous case

The phase diagram of the eBHM obtained from the SGMF is as shown in Fig. 1 for different values of V . It is important to note that here V is NN interaction which is V_1 of model

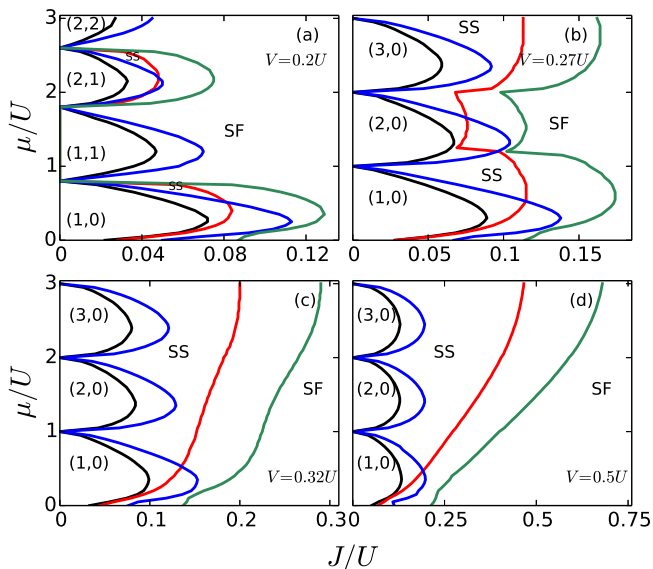


FIG. 2. The phase diagram of eBHM obtained from the CGMF theory with 2×2 clusters for uniform hopping amplitude ($J_x = J_y = J$) for $V/U = 0.2, 0.27, 0.32$, and 0.5 (a-d). The densities of the MI and DW phases are shown in the parenthesis. The plots show the phase boundaries for two cases $\alpha = 0$ and $\alpha = 1/2$. For the former case, the black line indicates the MI-SF or the DW-SS phase boundaries and the red line shows the SS-SF phase boundary. For the $\alpha = 1/2$ case, the blue line marks the MI-SF or DW-SS phase boundary and green line corresponds to the SS-SF boundary.

Eq. (2). We observed that for $zV < U$, where z is the coordination number of the system, the ground state alternates between MI and DW phases, and regions of SS phase occur as envelopes around the DW phase lobes. On increasing V , at a critical value $zV_c = U$ the MI lobes are transformed into DW phase. For $V \geq V_c$, the SS phase occupies a larger region in the phase diagram. As V is increased, the other observable effect is the critical value of J/U for the DW-SS transition also increases. At higher values, when $zV \gtrsim 1.5U$, the SS-SF phase boundary is like a linear function of the J , and this is discernible from Fig. 1(d). In particular, the phase boundary is linear when $zJ/U > 1$. These findings are in good agreement with the previous work of Iskin [60]. To examine the importance of the inter-site correlation effects the phase diagram using 2×2 CGMF method is as shown in Fig. 2. It is qualitatively similar to the one based on SGMF in Fig. 1. But, there are several quantitative differences. First, the MI and DW lobes are enhanced. For example, for $V/U = 0.2$ the tip of the DW(1,0) lobe is at $J/U = 0.071$ for $\alpha = 0$ with the SGMF theory. But, in the CGMF results it is increased to 0.072. Second, for all the values of V/U the SS-SF phase boundary starts at $J/U = 0$ and $\mu/U \approx 0$ with the SGMF theory. In the case of CGMF results, the SS-SF phase boundary starts at finite value of J/U and $\mu = 0$. This is even more prominent for $\alpha = 1/2$ and most evident with $V/U = 0.5$. Examining the plots in Fig. 2(d), we notice that the CGMF SS-SF phase boundary starts at $J/U = 0.213$ and $\mu = 0$. Third, the DW-SS and SS-SF phase boundaries are well sepa-

rated in the CGMF results. This is distinctly noticeable around the DW(2,0) lobe for $V/U = 0.27$. The two phase boundaries almost overlap in the SGMF results. But, in the CGMF results, as shown in Fig. 2(b), the closest approach of the two occurs at $\mu/U \approx 1.25$ and the two phase boundaries are separated by $\Delta J/U = 0.004$. And, finally, for higher values of V/U the SS-SF boundary is linear at higher μ with SGMF theory. But, it is curved with the CGMF theory.

As mentioned earlier, to study the effect of artificial gauge field, we choose $\alpha = 1/2$. So, hereafter *with artificial artificial gauge field* we mean $\alpha = 1/2$. And, *without artificial gauge field* means $\alpha = 0$. The artificial gauge field modifies the phase boundaries of MI, DW and SS, and the changes are discernible from the phase diagrams in Fig. 1. For example, for the (1,0) DW lobe with $V/U = 0.2$, the tip of the lobe is enhanced from $J/U \approx 0.071$ by 42% to 0.101 with artificial gauge field. Similarly, the tip of the SS lobe is enhanced from $J/U \approx 0.084$ to ≈ 0.119 , and these changes together implies a larger domain of SS phase surrounding the (1,0) DW phase. These changes arise from the localizing effect of the Landau quantization, associated with the artificial gauge field, on the itinerant bosons. In addition, there are major differences between the SGMF and CGMF phase diagrams. For example, the tip of the (1,0) DW lobe is increased from $J/U \approx 0.101$ in SGMF to $J/U \approx 0.113$ in CGMF. This implies that the effect of correlation due to finite magnetic flux is better captured by the CGMF method.

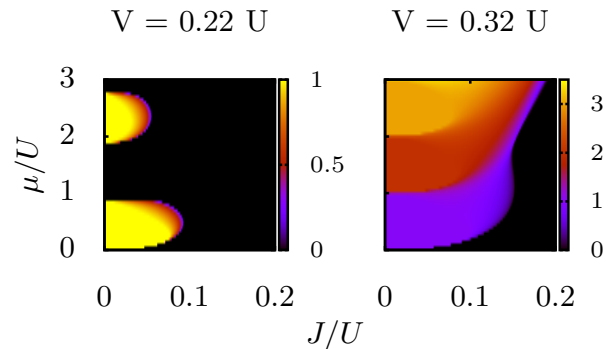


FIG. 3. The relative average occupancy of two consecutive sites are shown as a function of the chemical potential μ and hopping parameter J . The NN interaction is shown at the top of the figures.

The nature of the DW-SS transition is better represented by $\langle \Delta n \rangle$ and values for $V = 0.22U$ and $0.32U$ corresponding to $V < V_c$ and $V > V_c$ are shown in Fig. 3. In the figure, the dark regions correspond to MI and SF phases and the region in other colors correspond to DW and SS phases. For $V = 0.22U$, the regions in yellow color are DW phases and regions in other shades correspond to SS. The gradient in the shades indicates that the transition from DW to SS in terms of $\langle \Delta n \rangle$ is smooth. For the case of $V = 0.32U$, there are no dark regions in the neighbourhood of $J/U \approx 0$. This is due to the absence of MI lobes, and is consistent with the phase diagram shown in Fig. 1 as all the MI lobes are transformed to DW lobes. The nature of the DW phases are apparent and visible from color gradient in Fig. 3 as the colors indicate the difference in

the occupancy of two neighbouring lattice sites. Like in the case of $V = 0.22U$, regions with a color gradient indicate the SS phase and overall the relative average occupancy is in agreement with the phase diagram in Fig. 1. However, the phase diagram in terms of $\langle \Delta n \rangle$ provides a richer descriptions of the two phases, DW and SS, unique to the eBHM vis-a-vis BHM. And, the appropriate order parameter to examine the regions of SS phase.

B. Finite temperature effects

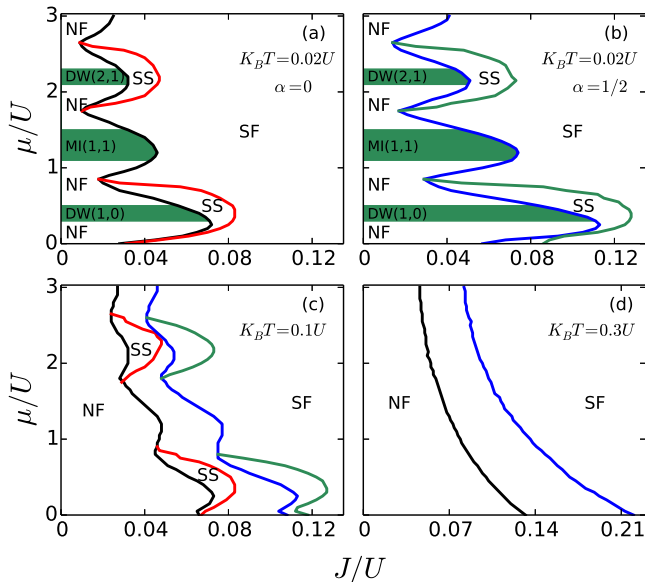


FIG. 4. The finite temperature phase diagram of eBHM obtained from CGMF theory with 2×2 clusters. The green striped region mark the DW and MI phases. (a) Phase diagram for $\alpha = 0$ at $k_B T = 0.02U$. The black line marks MI-SF, NF-SF, DW-SS, and NF-SS phase boundaries. And, the red line marks the SS-SF phase boundary. (b) Phase diagram for $\alpha = 1/2$ at $k_B T = 0.02U$. The blue line marks MI-SF, NF-SF, DW-SS, and NF-SS phase boundaries. And, the green line marks the SS-SF phase boundary. Phase diagrams for $\alpha = 0$ and $1/2$ at (c) $k_B T = 0.1U$ and (d) $k_B T = 0.3U$ with the combined color scheme of (a) and (b).

Thermal fluctuations associated with finite temperatures are an essential feature of experimental observations. Although the zero temperature phase diagrams do provide key insights and qualitative understanding, to relate with the experimental results it is essential to incorporate thermal fluctuations. We do this through the approach outlined in Section IID. As mentioned earlier, the SS phase is yet to be observed in the eBHM and this could be due to the sensitivity of the phase to the thermal fluctuations. At zero temperature, SS phase appears in the system at a finite value of the NN interaction V . In Fig. 4, we show the finite temperature phase diagram obtained using 2×2 clusters in the CGMF method. As we have demonstrated and by others [52–58] that the results with CGMF are more reliable, hereafter we only consider the results from CGMF theory. From the plots in Fig. 4, a distin-

guishing feature of the thermal fluctuations is the emergence of the NF phase. The thermal fluctuation melts both the MI and DW phases and destroys the SF phase at the MI-DW or DW-DW boundaries.

To be more specific at $k_B T = 0.02U$, as shown in Fig. 4(a-b), the green stripes mark the DW and MI phases and the NF phase exist outside of these. The MI and NF both have zero ϕ and commensurate densities. The difference is that the MI has integer commensurate density, but NF has real commensurate density. The DW phase, on the other hand, has checkerboard density but with integer values. So, density can effectively be used to differentiate these three phases, namely MI, DW and NF. On comparing the plots in Fig. 4(a) and Fig. 4(b), it is clear that the larger MI and DW lobes with finite α are retained at finite temperatures and hence the larger SS domain as well. At intermediate temperatures, both the MI and DW are entirely transformed into the NF phase but a portion of the SS lobes survives. This is visible in the phase diagram at $k_B T = 0.1U$ shown in the Fig. 4(c). From the plots in the figure, the quantitative differences with and without the artificial gauge field is also visible. With artificial gauge field, the domain of the NF and SS phases are larger. For example, at $\mu = 0$ the NF extends upto $J/U = 0.066$ and $J/U = 0.108$ for zero and finite α , respectively. This trend of larger extent of NF phase with finite α extends to higher values of μ . Upon further increase in temperature the crystalline order of the SS phase is destroyed and it vanishes from the phase diagram. At $k_B T \approx 0.3U$, as shown in Fig. 4(d), only the NF and SF phases are present in the system. At $\mu/U = 0$ the NF-SF phase boundary is located at $J/U = 0.132$ and $J/U = 0.220$ for zero and finite α , respectively. The separation between the location of the phase boundaries is reduced as μ/U increased. This is to be expected as the size of the DW lobes decrease with increasing μ/U .

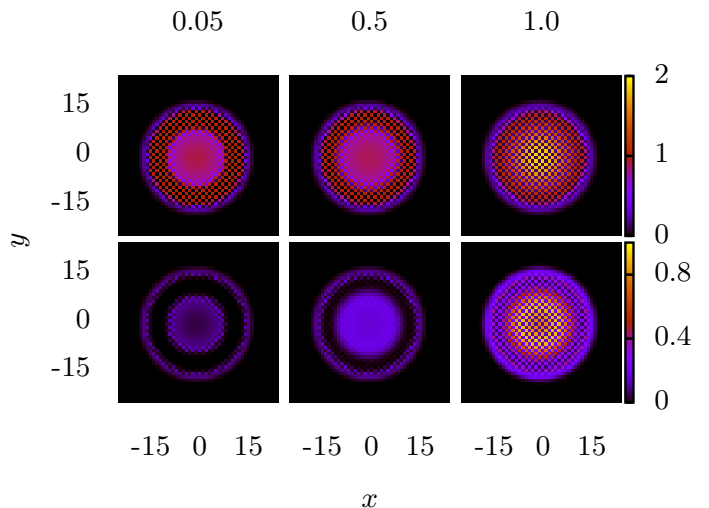


FIG. 5. The zero temperature density distribution (upper panel) and SF order parameter (lower panel) of a 50×50 square lattice for different values of dipolar interaction strengths V/U in V_{dip} model. The V/U value is shown at the top of the figures. Here x and y are in units of the lattice constant a .

C. Inhomogeneous case

The system considered so far is uniform and we emulate it with a 12×12 lattice with periodic boundary conditions. However, in most of the quantum gas experiments the optical lattice has a confining envelope potential. Most often the external envelope potential is a harmonic oscillator. Hence, the inhomogeneity arising from this confining potential is another factor to be considered for comparison with the experimental observations. Therefore, we examine the ground-state of eBHM in a 50×50 square lattice with SGMF theory. In which the external harmonic potential is incorporated in the chemical potential through the offset energy $\epsilon_{p,q} = \Omega(p^2 + q^2)$. Here Ω is the strength of the confining potential. The parameters of the system considered in the V_{dip} model are $J/V = 0.1$, $\mu/V = 2.8$ and $\Omega/V = 0.01$ [61]. The value of Ω is such that the atomic density outside the lattice potential is zero.

To determine the changes in the competing phases we examine the ground state of the system at $V/U = 0.05, 0.5,$ and 1.0 . These values cover the weak and strong limits of the dipolar interaction. In the experiments these regimes are reachable using Feshbach resonance in the dipolar atoms like Cr [62], Er [63] and Dy [64, 65]. Like in the previous cases, to study the effects of the thermal fluctuations we consider three different values of $k_B T/U = 0, 0.2,$ and 0.3 . At zero temperature profiles of $n_{p,q}$ and $\phi_{p,q}$ corresponding to $V/U = 0.05, 0.5,$ and 1.0 are shown in Fig. 5. For weak dipolar interaction $V/U = 0.05$ the density is nearly uniform in the central region. The corresponding $\phi_{p,q}$ though nearly uniform shows a dip around the center. But, it is more uniform at the intermediate strength of the dipole interaction $0.5 U$. In both of these cases, $V/U = 0.05$ and $0.5 U$, the central SF region is surrounded by the $(1, 0)$ DW phase and this is evident from ring-shaped profile of the checkerboard density pattern in the figure. The other key feature is that the domain of the DW phase gets narrowed as V/U is increased and above a critical value $V/U = 0.8$ there is a quantum phase transition from DW phase to SS phase. This happens when both the interaction strengths, on-site and dipole interactions are comparable. As shown in Fig. 5, for $V/U = 1$ there is a large region around the center where both the density and SF order parameter show checkerboard distributions. This is the signature of the SS phase.

Next, to relate to the experimental realizations we incorporate the finite temperature effects. For weak dipolar interaction the thermal fluctuations leads to the melting of the SF phase. This is evident from the density and SF order parameter corresponding to $V/U = 0.05$ at $k_B T/U = 0.2$ as shown in Fig. 6. A more detailed study, where V/U is fixed and temperature is changed, shows that the SF phase at the central region does exist at lower temperatures. But, it melts to NF phase at the critical temperature of $k_B T/U = 0.16$. At the higher value of $V/U = 0.5$ the central SF region reemerges and so does the SS phase at still higher value of $V/U = 1$. In short, with thermal fluctuations it is essential to have stronger dipolar interactions to observe SS phase. Considering the parameters of the experimental realization of dipolar condensates of ^{168}Er in optical lattices [44], the corresponding tem-

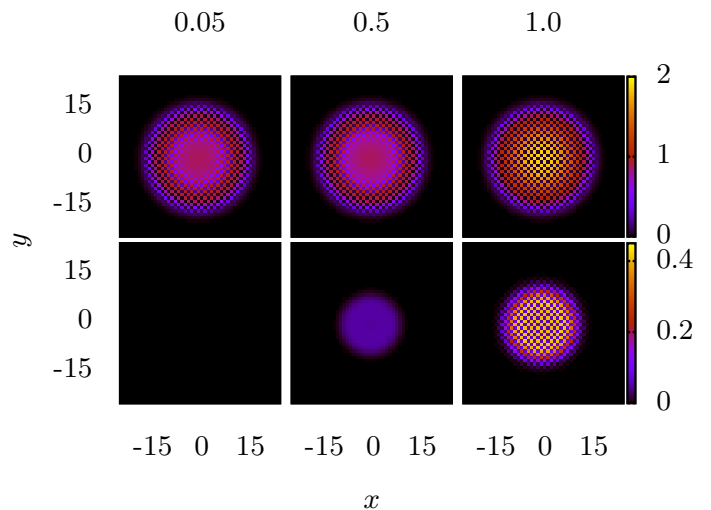


FIG. 6. The density distribution (upper panel) and SF order parameter (lower panel) of a 50×50 square lattice at $k_B T/U = 0.2$ for different values of dipolar strengths V/U in V_{dip} model. The V/U value is shown at the top of the figures. Here x and y are in units of the lattice constant a .

perature of $k_B T/U = 0.2$ is ≈ 40 nK. This is within the experimental realm and hence, the combined effect of dipolar interaction and artificial gauge field can lead to the emergence of SS phase within experimentally achievable parameter domain.

At higher temperatures, $k_B T/U \approx 0.3$, the central region is in NF phase for weaker dipole interactions $V/U \leq 0.5$. Then, on increasing V/U further the density assumes checkerboard pattern, but the SF order parameter is zero. That is the central region of the system is in the DW phase. This is to be compared and contrasted with the earlier result at $k_B T/U \approx 0.2$, where as shown in Fig. 6 the SS phase exists for $V/U = 1$. Thus, focusing on the strong interaction domain $V/U = 1$, our results show the existence of a SS-DW transition at $z k_B T = U$. In short, the SS phase exists in the system at lower temperatures, but the SS order melts into DW phase when $z k_B T \geq U$. On increasing the temperature further, the crystalline structure or diagonal long-range order of the DW phase starts to melt and at $z k_B T \approx 3 U$ system is fully in the NF phase. So, the melting of the SS phase occurs in two steps. First, the off-diagonal long-range SF order is destroyed. This transforms the SS phase into DW phase. And, second, the DW phase melts into NF phase. Like in the case of uniform system, there are no qualitative changes in the results with the introduction of artificial gauge field. However, the quantitative changes, which follows the same trends as in uniform system, can be important considerations in experimental realizations.

IV. CONCLUSIONS

We have examined the zero and finite temperature phase diagrams of eBHM in two dimensions using SGMF and CGMF

theory. In the presence of artificial gauge field the domain of SS phase is enhanced and 2×2 CGMF theory provide better description of the system. At higher temperatures, the thermal fluctuations destroys the SS phase and the phase diagram exhibits NF-SF transition. Furthermore, we have studied the system of dipolar atoms in the presence of a harmonic confinement as these atoms are predicted to stabilize the SS phase. Our results show that beyond a critical threshold of temperature $z k_B T \geq U$, the SS phase vanishes and the system is occupied by the DW phase. These suggest that the prospect of observing the SS phase is higher when the temperature $z k_B T < U$, this range of temperature is possible in the experiments of dipolar Bose gases loaded into optical

lattices. This offers an opportunity to observe SS phase in quantum dipolar gas experiments.

ACKNOWLEDGMENTS

The results presented in the paper are based on the computations using Vikram-100, the 100TFLOP HPC Cluster at Physical Research Laboratory, Ahmedabad, India. We thank Arko Roy, S. Gautam and S. A. Silotri for valuable discussions.

-
- [1] M. Lewenstein, A. Sanpera, V. Ahufinger, B. Damski, A. Sen(De), and U. Sen, "Ultracold atomic gases in optical lattices: mimicking condensed matter physics and beyond," *Adv. Phys.* **56**, 243 (2007).
- [2] I. Bloch, J. Dalibard, and W. Zwerger, "Many-body physics with ultracold gases," *Rev. Mod. Phys.* **80**, 885 (2008).
- [3] A. J. Leggett, "Can a solid be superfluid?" *Phys. Rev. Lett.* **25**, 1543 (1970).
- [4] G. V. Chester, "Speculations on Bose-Einstein condensation and quantum crystals," *Phys. Rev. A* **2**, 256 (1970).
- [5] A. F. Andreev and I. M. Lifshitz, "Quantum theory of defects in crystals," *Sov. Phys. JETP* **29**, 1107 (1969).
- [6] D. J. Thouless, "The flow of a dense superfluid," *Ann. Phys.* **52**, 403 (1969).
- [7] E. Kim and M. H. W. Chan, "Probable observation of a supersolid helium phase," *Nature (London)* **427**, 225 (2004).
- [8] E. Kim and M. H. W. Chan, "Observation of superflow in solid helium," *Science* **305**, 1941 (2004).
- [9] D. Y. Kim and M. H. W. Chan, "Absence of supersolidity in solid helium in porous vycor glass," *Phys. Rev. Lett.* **109**, 155301 (2012).
- [10] J. Lonard, A. Morales, P. Zupancic, T. Esslinger, and T. Donner, "Supersolid formation in a quantum gas breaking a continuous translational symmetry," *Nature (London)* **543**, 87 (2017).
- [11] J.-R. Li, J. Lee, W. Huang, S. Burchesky, B. Shteynas, F. Top, A. O. Jamison, and W. Ketterle, "A stripe phase with supersolid properties in spin-orbit-coupled Bose-Einstein condensates," *Nature (London)* **543**, 91 (2017).
- [12] L. Tanzi, E. Lucioni, F. Famà, J. Catani, A. Fioretti, C. Gabbanini, R. N. Bisset, L. Santos, and G. Modugno, "Observation of a dipolar quantum gas with metastable supersolid properties," *Phys. Rev. Lett.* **122**, 130405 (2019).
- [13] F. Böttcher, J.-N. Schmidt, M. Wenzel, J. Hertkorn, M. Guo, T. Langen, and T. Pfau, "Transient supersolid properties in an array of dipolar quantum droplets," *Phys. Rev. X* **9**, 011051 (2019).
- [14] L. Chomaz, D. Petter, P. Ilzhöfer, G. Natale, A. Trautmann, C. Politi, G. Durastante, R. M. W. van Bijnen, A. Patscheider, M. Sohmen, M. J. Mark, and F. Ferlaino, "Long-lived and transient supersolid behaviors in dipolar quantum gases," *Phys. Rev. X* **9**, 021012 (2019).
- [15] R. Landig, L. Hruby, N. Dogra, M. Landini, R. Mottl, T. Donner, and T. Esslinger, "Quantum phases from competing short- and long-range interactions in an optical lattice," *Nature (London)* **532**, 476 (2016).
- [16] T. Flottat, L. de Forges de Parny, F. Hébert, V. G. Rousseau, and G. G. Batrouni, "Phase diagram of bosons in a two-dimensional optical lattice with infinite-range cavity-mediated interactions," *Phys. Rev. B* **95**, 144501 (2017).
- [17] G. G. Batrouni and R. T. Scalettar, "Phase separation in supersolids," *Phys. Rev. Lett.* **84**, 1599 (2000).
- [18] L. Dang, M. Boninsegni, and L. Pollet, "Vacancy supersolid of hard-core bosons on the square lattice," *Phys. Rev. B* **78**, 132512 (2008).
- [19] S. Wessel, "Phase diagram of interacting bosons on the honeycomb lattice," *Phys. Rev. B* **75**, 174301 (2007).
- [20] J. Y. Gan, Y. C. Wen, J. Ye, T. Li, S.-J. Yang, and Y. Yu, "Extended Bose-Hubbard model on a honeycomb lattice," *Phys. Rev. B* **75**, 214509 (2007).
- [21] P. Sengupta, L. P. Pryadko, F. Alet, M. Troyer, and G. Schmid, "Supersolids versus phase separation in two-dimensional lattice bosons," *Phys. Rev. Lett.* **94**, 207202 (2005).
- [22] B. Capogrosso-Sansone, C. Trefzger, M. Lewenstein, P. Zoller, and G. Pupillo, "Quantum phases of cold polar molecules in 2D optical lattices," *Phys. Rev. Lett.* **104**, 125301 (2010).
- [23] T. Ohgoe, T. Suzuki, and N. Kawashima, "Novel mechanism of supersolid of ultracold polar molecules in optical lattices," *J. Phys. Soc. Jpn.* **80**, 113001 (2011).
- [24] Y.-H. Chan, Y.-J. Han, and L.-M. Duan, "Supersolid and charge-density-wave states from anisotropic interaction in an optical lattice," *Phys. Rev. A* **82**, 053607 (2010).
- [25] T. Ohgoe, T. Suzuki, and N. Kawashima, "Quantum phases of hard-core bosons on two-dimensional lattices with anisotropic dipole-dipole interaction," *Phys. Rev. A* **86**, 063635 (2012).
- [26] L. Mathey, I. Danshita, and C. W. Clark, "Creating a supersolid in one-dimensional Bose mixtures," *Phys. Rev. A* **79**, 011602 (2009).
- [27] G. G. Batrouni, F. Hébert, and R. T. Scalettar, "Supersolid phases in the one-dimensional extended soft-core bosonic Hubbard model," *Phys. Rev. Lett.* **97**, 087209 (2006).
- [28] K. Góral, L. Santos, and M. Lewenstein, "Quantum phases of dipolar bosons in optical lattices," *Phys. Rev. Lett.* **88**, 170406 (2002).
- [29] V. W. Scarola and S. Das Sarma, "Quantum phases of the extended Bose-Hubbard Hamiltonian: Possibility of a supersolid state of cold atoms in optical lattices," *Phys. Rev. Lett.* **95**, 033003 (2005).
- [30] S. Yi, T. Li, and C. P. Sun, "Novel quantum phases of dipolar Bose gases in optical lattices," *Phys. Rev. Lett.* **98**, 260405 (2007).

- [31] K.-K. Ng and Y.-C. Chen, “Supersolid phases in the bosonic extended Hubbard model,” *Phys. Rev. B* **77**, 052506 (2008).
- [32] S. Wessel and M. Troyer, “Supersolid hard-core bosons on the triangular lattice,” *Phys. Rev. Lett.* **95**, 127205 (2005).
- [33] D. Heidarian and K. Damle, “Persistent supersolid phase of hard-core bosons on the triangular lattice,” *Phys. Rev. Lett.* **95**, 127206 (2005).
- [34] R. G. Melko, A. Paramekanti, A. A. Burkov, A. Vishwanath, D. N. Sheng, and L. Balents, “Supersolid order from disorder: Hard-core bosons on the triangular lattice,” *Phys. Rev. Lett.* **95**, 127207 (2005).
- [35] M. Boninsegni and N. Prokof’ev, “Supersolid phase of hard-core bosons on a triangular lattice,” *Phys. Rev. Lett.* **95**, 237204 (2005).
- [36] A. Sen, P. Dutt, K. Damle, and R. Moessner, “Variational wave-function study of the triangular lattice supersolid,” *Phys. Rev. Lett.* **100**, 147204 (2008).
- [37] D. Yamamoto, I. Danshita, and C. A. R. Sá de Melo, “Dipolar bosons in triangular optical lattices: Quantum phase transitions and anomalous hysteresis,” *Phys. Rev. A* **85**, 021601 (2012).
- [38] S. V. Isakov, S. Wessel, R. G. Melko, K. Sengupta, and Y. B. Kim, “Hard-core bosons on the kagome lattice: Valence-bond solids and their quantum melting,” *Phys. Rev. Lett.* **97**, 147202 (2006).
- [39] C. Trefzger, C. Menotti, and M. Lewenstein, “Pair-supersolid phase in a bilayer system of dipolar lattice bosons,” *Phys. Rev. Lett.* **103**, 035304 (2009).
- [40] K. Yamamoto, S. Todo, and S. Miyashita, “Successive phase transitions at finite temperatures toward the supersolid state in a three-dimensional extended Bose-Hubbard model,” *Phys. Rev. B* **79**, 094503 (2009).
- [41] B. Xi, F. Ye, W. Chen, F. Zhang, and G. Su, “Global phase diagram of three-dimensional extended boson Hubbard model: A continuous-time quantum Monte Carlo study,” *Phys. Rev. B* **84**, 054512 (2011).
- [42] T. Ohgoe, T. Suzuki, and N. Kawashima, “Commensurate supersolid of three-dimensional lattice bosons,” *Phys. Rev. Lett.* **108**, 185302 (2012).
- [43] B. Pasquiou, G. Bismut, E. Maréchal, P. Pedri, L. Vernac, O. Gorceix, and B. Laburthe-Tolra, “Spin relaxation and band excitation of a dipolar Bose-Einstein condensate in 2d optical lattices,” *Phys. Rev. Lett.* **106**, 015301 (2011).
- [44] S. Baier, M. J. Mark, D. Petter, K. Aikawa, L. Chomaz, Z. Cai, M. Baranov, P. Zoller, and F. Ferlaino, “Extended Bose-Hubbard models with ultracold magnetic atoms,” *Science* **352**, 201 (2016).
- [45] M. Aidelsburger, M. Atala, S. Nascimbène, S. Trotzky, Y.-A. Chen, and I. Bloch, “Experimental realization of strong effective magnetic fields in an optical lattice,” *Phys. Rev. Lett.* **107**, 255301 (2011).
- [46] H. Miyake, G. A. Siviloglou, C. J. Kennedy, W. C. Burton, and W. Ketterle, “Realizing the Harper Hamiltonian with laser-assisted tunneling in optical lattices,” *Phys. Rev. Lett.* **111**, 185302 (2013).
- [47] M. Atala, M. Aidelsburger, M. Lohse, J. T. Barreiro, B. Paredes, and I. Bloch, “Observation of chiral currents with ultracold atoms in bosonic ladders,” *Nature (London)* **10**, 588 (2014).
- [48] C. J. Kennedy, W. C. Burton, W. C. Chung, and W. Ketterle, “Observation of Bose-Einstein condensation in a strong synthetic magnetic field,” *Nature (London)* **11**, 859 (2015).
- [49] D. S. Rokhsar and B. G. Kotliar, “Gutzwiller projection for bosons,” *Phys. Rev. B* **44**, 10328 (1991).
- [50] W. Krauth, M. Caffarel, and J.-P. Bouchaud, “Gutzwiller wave function for a model of strongly interacting bosons,” *Phys. Rev. B* **45**, 3137 (1992).
- [51] K. Sheshadri, H. R. Krishnamurthy, R. Pandit, and T. V. Ramakrishnan, “Superfluid and insulating phases in an interacting-boson model: Mean-field theory and the RPA,” *EPL* **22**, 257 (1993).
- [52] P. Buonsante, V. Penna, and A. Vezzani, “Fractional-filling loop-hole insulator domains for ultracold bosons in optical superlattices,” *Phys. Rev. A* **70**, 061603 (2004).
- [53] D. Yamamoto, “Correlated cluster mean-field theory for spin systems,” *Phys. Rev. B* **79**, 144427 (2009).
- [54] P. Pisarski, R. M. Jones, and R. J. Gooding, “Application of a multisite mean-field theory to the disordered Bose-Hubbard model,” *Phys. Rev. A* **83**, 053608 (2011).
- [55] T. McIntosh, P. Pisarski, R. J. Gooding, and E. Zaremba, “Multisite mean-field theory for cold bosonic atoms in optical lattices,” *Phys. Rev. A* **86**, 013623 (2012).
- [56] D.-S. Lühmann, “Cluster Gutzwiller method for bosonic lattice systems,” *Phys. Rev. A* **87**, 043619 (2013).
- [57] R. Bai, S. Bandyopadhyay, S. Pal, K. Suthar, and D. Angom, “Bosonic quantum Hall states in single-layer two-dimensional optical lattices,” *Phys. Rev. A* **98**, 023606 (2018).
- [58] S. Pal, R. Bai, S. Bandyopadhyay, K. Suthar, and D. Angom, “Enhancement of Bose glass phase in presence of artificial gauge field,” accepted for publication in *Phys. Rev. A*, arxiv:1807.00269 (2019).
- [59] M. Greiner, O. Mandel, T. Esslinger, T. W. Hansch, and I. Bloch, “Quantum phase transition from a superfluid to a Mott insulator in a gas of ultracold atoms,” *Nature (London)* **415**, 39 (2002).
- [60] M. Iskin, “Route to supersolidity for the extended Bose-Hubbard model,” *Phys. Rev. A* **83**, 051606 (2011).
- [61] C. Trefzger, C. Menotti, and M. Lewenstein, “Ultracold dipolar gas in an optical lattice: The fate of metastable states,” *Phys. Rev. A* **78**, 043604 (2008).
- [62] J. Werner, A. Griesmaier, S. Hensler, J. Stuhler, T. Pfau, A. Simoni, and E. Tiesinga, “Observation of Feshbach resonances in an ultracold gas of ^{52}Cr ,” *Phys. Rev. Lett.* **94**, 183201 (2005).
- [63] A. Frisch, M. Mark, K. Aikawa, F. Ferlaino, J. L. Bohn, C. Makrides, A. Petrov, and S. Kotochigova, “Quantum chaos in ultracold collisions of gas-phase erbium atoms,” *Nature (London)* **507**, 475 (2014).
- [64] T. Maier, I. Ferrier-Barbut, H. Kadau, M. Schmitt, M. Wenzel, C. Wink, T. Pfau, K. Jachymski, and P. S. Julienne, “Broad universal Feshbach resonances in the chaotic spectrum of dysprosium atoms,” *Phys. Rev. A* **92**, 060702 (2015).
- [65] E. Lucioni, L. Tanzi, A. Fregosi, J. Catani, S. Gozzini, M. Inguscio, A. Fioretti, C. Gabbanini, and G. Modugno, “Dysprosium dipolar Bose-Einstein condensate with broad Feshbach resonances,” *Phys. Rev. A* **97**, 060701 (2018).